# Sound speed and attenuation in water-saturated glass beads as a function of frequency and porosity

Theodore F. Argo IV, Matthew D. Guild, and Preston S. Wilson

*Dept. Mech. Eng. and Applied Res. Labs.; The Univ. of Texas at Austin*

*P.O. Box 8029; Austin TX 78713-8029*

Matthias Schröter

*Max Planck Institute for Dynamics and Self-Organization*

*Bunsenstraße 10; 37073 Göttingen,*

*Germany*

Charles Radin

*Department of Mathematics,*

*The University of Texas at Austin,*

*1 University Station C1200; Austin TX 78712*

Harry L. Swinney

*Center for Nonlinear Dynamics and Department of Physics,*

*The University of Texas at Austin,*

*1 University Station C1610; Austin TX 78712*

(Dated: June 25, 2009)

**Abstract**

Sound propagation in water-saturated granular sediments is known to depend on the sediment porosity, but few data in the literature address both the frequency and porosity dependency. To begin to address this deficiency, a fluidized bed technique was used to control the porosity of an artificial sediment composed of 265 $\mu$m-diameter glass spheres. Time-of-flight measurements and the Fourier phase technique were utilized to determine the sound speed and attenuation for frequencies from 300 kHz to 800 kHz, and porosities from 0.37 to 0.43. A Biot-based model qualitatively describes the porosity dependence, but a transition to a scattering-dominated regime is also observed.

PACS numbers: 43.30.Ma, 43.35.Bf

## I. INTRODUCTION

Numerous models have been proposed to describe sound propagation in water saturated granular materials (see Refs. [1, 2, 3, 4, 5] for a sampling); however, no model yet accurately describes both the sound speed and attenuation in these materials across the full range of frequencies of interest in underwater acoustics. Measurements of the acoustic properties of water saturated sediments have been made under a variety of conditions including *in situ* measurements,[6,7] retrieved samples,[7,8] reconstituted samples,[9,10] and artificial sediments.[11] There is a large variability in the observed sound speeds and attenuation coefficients of these various sediments due to the wide range of porosities, permeabilities, and other physical properties they exhibit. Richardson and Jackson have studied the effect of porosity on a global scale, compiling numerous measurements obtained across many sediment types.[12] Naturally, the sediment porosity changes are also accompanied by grain size and material differences.

In none of these studies, nor in any other studies known to the authors, was the effect of porosity studied in a controlled manner across a range of frequencies, for a single sediment sample with uniform grain size distribution. In such an idealized case, one can focus on the effect of porosity in isolation, and with sufficient knowledge of most of the sediment physical parameters, one can make meaningful comparisons to various models of sound propagation. Towards this end, a fluidized bed apparatus was used to prepare specific porosities of a spherical glass bead sediment, and ultrasonic time-of-flight measurements were obtained. Experimental results were compared to the predictions of the Williams effective density fluid model.[13] The purpose of this brief communication is to describe the porosity-control technique as applied to sediment acoustics and to present a set of example measurements.

## II. DESCRIPTION OF EXPERIMENT

The artificial sediment was composed of 265 $\mu$m $\pm$15 $\mu$m diameter soda lime glass spheres saturated with degassed distilled water. The beads were sorted using a sieve shaker

between 250 $\mu$m and 280 $\mu$m fine mesh sieves. The mass of the dry spheres was measured, and the spheres were then added to the apparatus shown in Fig. 1. Degassed distilled water was then continuously pumped through the sample for 30 minutes and then allowed to rest overnight to dissolve trapped gas bubbles.

Sediment porosity $\beta$ was controlled by using the fluidized bed apparatus shown in Fig. 1, which is similar to that described by Schröter *et al.*[14,15] The interior of the sample holder was 6 cm $\times$ 6 cm square and 30 cm tall, with the sediment height dependent upon porosity, but nominally 100 mm. Two parallel polycarbonate walls of the sample holder were 1 mm thick and the opposite two were 10 mm thick. Control of the porosity of the monodisperse fluid-saturated bead pack is initiated by pumping water at a particular flow rate through the distributor (a block of sintered bronze powder, 5 mm thick with approximately 10 $\mu$m-diameter pores). The beads are carried into suspension, with the overall magnitude of their motion governed by the flow rate. The beads achieve steady-state motion and after two minutes, the flow is stopped. The beads are then given one minute to settle. The resulting porosity is dependent upon the flow rate. An additional procedure was use to achieve uniform porosity for $\beta < 0.40$: A series of flow pulses were introduced, starting at a high flow rate but with an incrementally decreasing flow rate. This allowed the bead column to settle more uniformly.

A rectangular excitation pulse with a 10 volt amplitude and a 1.25 $\mu$s width was directed to a pair of broadband ultrasonic transducers (labeled Tx) with center frequencies of 500 kHz, which transmitted simultaneously through the water and sediment paths, as shown in Fig. 1. Another pair of ultrasonic transducers (labeled Rx) with center frequencies of 550 kHz received the acoustic signals. Commercially-available ultrasonic coupling gel was used between the transducer faces and the sample holder walls. A digital storage oscilloscope acquired both the source signal and the received signals. In all cases, 512 linear time-domain signals were averaged onboard the scope to remove noise. The averaged signals were transferred to a computer for analysis.

To determine sediment porosity, images of the beads were obtained with a digital camera

at the same time as the acoustic measurements. A fiducial scale indicating sediment height $h$ was placed within the field of view of the camera. The porosity of the sample $\beta$ was determined with $\beta = 1 - m_\mathrm{b}/\left(\rho_\mathrm{b} h A\right)$, where $m_\mathrm{b}$ and $\rho_\mathrm{b}$ are the dry mass and density of the beads, $h$ is the height of the beads within the column, and $A$ is the cross-sectional area of the column. A resistance temperature detector, labled RTD in Fig. 1, was used to measure the temperature during the acoustic measurements. Equation 5.6.8 of Ref. [16] was later used to determine the sound speed $c_0$ of the distilled water at the experimental temperature.

The apparatus and preparation technique described above yielded a uniform porosity throughout the sample,[14,15] but also resulted in an acoustic path length that was shorter than desired. Increasing the cross-sectional area of the apparatus while retaining a homogeneous porosity is difficult. Since the goal of this work was to investigate the effect of porosity, we chose to achieve a homogeneous sediment at the expense of simplicity in the acoustic data analysis. In addition, the porosity control procedure can take as long as several hours for the dense sediments. Because the water temperature follows temperature fluctuations in the laboratory, there could be significant temperature-depenent sound speed changes in the sample before and after the procedure. Hence, the four-transducer apparatus of Fig. 1 was used to facilitate contemporaneous post-preparation water-path calibration and sediment-path measurements.

Since the path length was short, on the order of a few wavelengths at the lowest frequencies, coupling between the sediment sample and the tank walls and transducers was found to be significant, and the short path length increased error due to uncertainty in path length and path length differences. The coupling effect is demonstrated in Fig. 2, which shows the phase of the measured electrical input impedance of one of the receiving acoustic transducers when mounted in the apparatus filled only with water, and when filled with water-saturated beads. There is as much as a thirty degree phase difference between these two cases. Further, initial measurements with distilled water revealed that the sound speed and attenuation determined by Eqs. 1 and 2 applied to the present four-transducer apparatus included a systematic error due to a small path length difference between the two

transducer pairs. The effect of these systematic errors was found to be the same order of magnitude (a few percent) as the sound speed changes expected from the porosity dependency. Therefore, the calibration and error correction procedure described in Section III was implemented. Near-field effects were quantified as described in Ref. [17] and found to be insignificant, which was also the case for a similar experiment described in Ref. [10].

## III. ANALYSIS

The Fast Fourier Transforms (FFTs) of the received signals for both the water-paths and sediment-paths were calculated. A Fourier phase technique[18] was then used to obtain a measurement of the apparent sound speed $c_{\text{sys}}$ of the sediment within the experimental system. This sound speed was calculated with

$$c_{\text{sys}} = c_0 \left[ 1 - \frac{c_0 \Delta\phi}{l\omega} \right]^{-1}, \tag{1}$$

where $c_0$ was the sound speed in the water portion of the fluidized bed determined by Eq. 5.6.8 of Ref. [16], $l$ was the length of travel for the acoustic wave within the sample, $\omega = 2\pi f$ was the angular frequency, and $\Delta\phi$ was the difference in phase between the two FFT spectra at frequency $\omega$. The apparent frequency dependent attenuation of the sediment within the system was calculated with

$$\alpha_{\text{sys}} = \frac{20}{l} \log_{10} \left( \frac{A_0}{A_{\text{sys}}} \right), \tag{2}$$

where $A_0$ and $A_{\text{sys}}$ were the frequency dependent magnitudes of the FFT at frequency $\omega$ for the water and sediment paths, respectively.

An equivalent circuit transmission line model of the experimental system (Fig. 3a) was used to correct for the systematic errors described in Sec. II. The model included the transducers, coupling gel, tank walls, and the sediment (or water). The passive layers (Fig. 3c) were modeled with $Z_0^{(n)} = \rho^{(n)} c^{(n)} S^{(n)}/N^2$, $Z_1^{(n)} = jZ_0^{(n)} \tan\left[k^{(n)} l^{(n)}/2\right]$, and $Z_2^{(n)} = -jZ_0^{(n)}/\sin\left[k^{(n)} l^{(n)}\right]$, where $k^{(n)}$, $\rho^{(n)}$, and $c^{(n)}$ are the wave number, density, and sound speed within the $n$th component respectively, $l^{(n)}$ is the path length in the $n$th component,

$S^{(n)}$ is the surface area, and $N$ is the transformation factor from one physical domain to another. The values of the sediment sound speed and attenuation used in the system model are denoted by $c_{\text{sed}}$ and $\alpha_{\text{sed}}$, respectively, and are used to construct both $k$ and $c$ for the sediment layer. A Mason equivalent circuit model of a thickness mode piezoelectric resonator with a matching layer[19] was used to model the transducers (Fig. 3b). The unloaded electrical impedance of each transducer was measured and the values for each model element shown in Fig. 3b were found by fitting the model to the impedance measurement, including the use of the properties for PZT-IV listed in Table 4.3 of Ref. [20]. Additional material properties for the model elements are listed in Table I. Measurements made with distilled degassed water occupying both transmission paths allowed for calibration of the transmission path lengths in the model.

To perform the correction, the experimental input signals for the water and sediment paths were digitized, FFTs were taken, the resulting spectra were input into the system model, and the output spectra were calculated. These modeled output spectra were then subjected to the calculations described in Eqs. 1 and 2, which yield modeled system values of $c_{\text{sys,m}}$ and $\alpha_{\text{sys,m}}$. Using Newton-Raphson iteration, $c_{\text{sed}}$ and $\alpha_{\text{sed}}$ were systematically varied in the model until the modeled system values $c_{\text{sys,m}}$ and $\alpha_{\text{sys,m}}$ matched the measured values of $c_{\text{sys}}$ and $\alpha_{\text{sys}}$ for each frequency $\omega$ and for each porosity. The values of $c_{\text{sed}}$ and $\alpha_{\text{sed}}$ that achieve this match were taken to be the free-field sound speeds and attenuation coefficients of the sediment samples and are reported in Fig. 4.

## IV. RESULTS

In Fig. 4a and b, the frequency dependence of the corrected sound speed and attenuation measurements are compared to the predictions of the Effective Density Fluid Model (EDFM),[13] for the parameters given in Table II. Negative dispersion is apparent in Fig. 4a for all porosities above 550 kHz. Considering just one frequency, say 600 kHz, the variation in the measured sound speed as a function of porosity is well-predicted by the EDFM.

Measured values of the attenuation in Fig. 4b are an order of magnitude greater than the predictions of the EDFM, however this discrepancy is consistent with other measurements reported in the literature.[10,11,21] Trendlines with frequency $f^{1/2}$ and $f^4$ dependance are also shown. At low frequencies, the data are described by an $f^{1/2}$ dependence as predicted by Biot theory. The sharp increase in attenuation to an $f^4$ dependence at frequencies above 700 kHz is attributable to scattering effects.[2,10,22]

In Figs. 4c and d, the porosity dependence of the measured sound speed and attenuation are shown and compared to the predictions of the EDFM at three frequencies. Measurements at porosities not shown in Fig. 4a and b are shown here. It is apparent that the EDFM does a good job of describing the observed relative porosity dependence. Note that all of the sound speeds predicted by the EDFM nearly collapse onto a single line. The negative dispersion exhibited by the measured sound speed remains apparent. Plotted this way, the sound speed monotonically decreases with porosity, while the attenuation is nearly constant. Therefore, the porosity appears to be a good indicator of the sound speed but a poor indicator of the attenuation in this glass bead sediment.

## V. CONCLUSION

The porosity- and frequency-dependent sound speed and attenuation in an artificial water-saturated glass bead sediment were measured using a fluidized bed apparatus with a time-of-flight acoustic measurement and a Fourier phase technique. The relative dependence of the sound speed and attenuation on porosity is properly predicted by the Biot-based EDFM model throughout the experimental frequency range, 300 kHz to 800 kHz, and it also quantitatively described the sound speed ratio to within about $\pm 1\%$. The measured frequency dependence reveals negative dispersion at frequencies above 550 kHz. The predicted and the measured attenuation is proportional to $f^{1/2}$ below 700 kHz, but the measured attenuation exhibits an $f^4$ proportionality at higher frequencies for all porosities. The EDFM underpredicts the absolute value of the attenuation throughout the frequency range,

but it is not intended to be accurate at the highest frequencies in this work. The authors acknowledge that other models[2,11,21] will likely do a better job predicting the dispersion and attenuation in this frequency range, but no current model can transition from $f^{1/2}$ to $f^4$ frequency dependence. The present purpose is to report the porosity control technique and initial measurements obtained with it, including the observation of the transition into the scattering-controlled regime. Measurements with a variety of bead sizes and with natural sand grains, and a more thorough model evaluation are currently underway.

## Acknowledgments

This work was supported by the Office of Naval Research Ocean Acoustics Office, the Robert A. Welch Foundation Grant F-0805, and National Science Foundation Grant DMS-0700120. The authors also wish to acknowledge Nicholas P. Chotiros for insightful discussions and Udo Krafft for experimental support.

## References

[1] M. A. Biot, "Generalized theory of acoustic propagation in porous dissipative media", J. Acoust. Soc. Am. **34**, 1254–1264 (1962).

[2] L. Schwartz and T. J. Plona, "Ultrasonic propagation in close-packed disordered suspensions", J. App. Physics **55**, 3971–3977 (1984).

[3] R. D. Stoll, *Sediment Acoustics* (Springer-Verlag, New York, 1989).

[4] M. J. Buckingham, "Theory of compressional and shear waves in fluidlike marine sediments", J. Acoust. Soc. Am. **103**, 288–299 (1998).

[5] N. P. Chotiros and M. J. Isakson, "A broadband model of sandy ocean sediments: Biot-Stoll with contact squirt flow and shear drag", J. Acoust. Soc. Am. **116**, 2011–2022 (2004).

[6] A. Turgut and T. Yamamoto, "Measurements of acoustic wave velocities and attenuation in marine sediments", J. Acoust. Soc. Am. **87**, 2376–2383 (1990).

[7] K. L. Williams, D. R. Jackson, E. I. Thorsos, D. Tang, and S. G. Schock, "Comparison of sound speed and attenuation measured in a sandy sediment to predictions based on the Biot theory of porous media", IEEE Journal of Oceanic Engineering **27**, 413–428 (2002).

[8] E. L. Hamilton and R. T. Bachman, "Sound velocity and related properties of marine sediments", J. Acoust. Soc. Am. **72**, 1891–1904 (1982).

[9] D. J. Shirley and L. D. Hampton, "Shear-wave measurements in laboratory sediments", J. Acoust. Soc. Am. **63**, 607–613 (1978).

[10] K. I. Lee, V. F. Humphrey, B.-N. Kim, and S. W. Yoon, "Frequency dependancies of phase velocity and attenuation coefficient in a water-saturated sandy sediment from 0.3 to 1.0 MHz", J. Acoust. Soc. Am. **121**, 2553–2558 (2007).

[11] B. T. Hefner and K. L. Williams, "Sound speed and attenuation measurements in unconsolidated glass-bead sediments saturated with viscous pore fluids", J. Acoust. Soc. Am. **120**, 2538–2549 (2006).

[12] D. R. Jackson and M. D. Richardson, *High Frequency Seafloor Acoustics* (Springer Science, New York, 2007).

[13] K. L. Williams, "An effective density fluid model for acoustic propagation in sediments derived from Biot theory", J. Acoust. Soc. Am. **110**, 2276–2281 (2001).

[14] M. Schröter, D. I. Goldman, and H. L. Swinney, "Stationary state fluctuations in a granular medium", Physical Review E **71**, 030301(R) (2005).

[15] M. Schröter, S. Nägle, C. Radin, and H. L. Swinney, "Phase transition in a static granular system", Europhysics Letters **78**, 44004 (2007).

[16] L. E. Kinsler, A. R. Frey, A. B. Coppens, and J. V. Sanders, *Fundamentals of Acoustics*, 4th edition (Wiley, New York, 1999).

[17] W. Xu and J. J. Kaufman, "Diffraction correction methods for insertion ultrasound attenuation estimation", IEEE Transactions on Biomedical Engineering **40**, 563–570 (1993).

[18] J. B. Molyneux and D. R. Schmitt, "Compressional-wave velocities in attenuating media: a laboratory physical model study", Geophysics **65**, 1162–1167 (2000).

[19] W. P. Mason, *Physical Acoustics and the Properties of Solids* (Van Nostrand, Princeton,

NJ, 1958).

[20] O. B. Wilson, *Introduction to the Theory and Design of Sonar Transducers* (Peninsula, Los Altos, California, 1988).

[21] N. P. Chotiros and M. J. Isakson, "High-frequency dispersion from viscous drag at the grain-grain contact in water-saturated sand", J. Acoust. Soc. Am. **124**, EL296–EL301 (2008).

[22] J. H. Page, P. Sheng, H. P. Schriemer, I. Jones, X. Jing, and D. A. Weitz, "Group velocity in strongly scattering media", Science **271**, 634–637 (1996).

[23] A. Kadaksham, S. B. Pillapakkam, and P. Singh, "Permeability of periodic arrays of spheres", Mechanics Research Communications **32**, 659–665 (2005).

[24] R. Dias, J. A. Teixeira, M. Mota, and A. Yelshin, "Tortuosity variation in a low density binary particulate bed", Separation and Purification Technology **51**, 180–184 (2006).

[25] V. Batu, *Aquifer Hydraulics: A Comprehensive Guide to Hydrogeologic Data Analysis* (John Wiley, New York, 1998).

| | density ($kg/m^3$) | sound speed (m/s) |
|---|---|---|
| matching layer | 1200 | $2650\,(1 + 0.01j)$ |
| coupling gel | 1000 | 1500 |
| sample holder wall | 1200 | $1800\,(1 + 0.01j)$ |

TABLE I. Parameters used in the transmission line model. The sound speed and density of the transducer matching layers and coupling gel were obtained from their respective manufacturers. The sample holder wall density was measured, and its sound speed was also measured using commercial ultrasonic testing instrumentation.

| | | | |
|---|---|---|---|
| grain density | 2487 kg/m$^3$ | water density | 998 kg/m$^3$ |
| bead bulk mod. | 41.175 GPa | water sound vel. (m/s) | 1474, 1472, 1471, 1472 |
| water viscosity | 0.001 Pa·s | permeability (m$^{-2}$) | [5.32, 6.44, 7.50, 8.87]$\times 10^{-11}$ |
| tortuosity | 1.63, 1.59, 1.57, 1.54 | porosity | 0.376, 0.393, 0.407, 0.423 |

TABLE II. Parameters used as inputs to the Williams EDFM model.[13] Grain density was measured using a Gay-Lussac flask. Water sound speed was given by Eq. 5.6.8 in Ref. [16]. Tortuosity was calculated using Ref. [24] with an exponent of 0.5. Permeability was calculated using the Kozeny-Carman Equation[25] with a coefficient of 5 and the pore size factor given by Ref. [13]. Bead bulk modulus was taken from the manufacturer's specification. Porosity was determined by the method in Sec. II. When multiple entries appear within a cell, they are for the four porosities that are tabulated here, respectively, and that also appear in frames (a) and (b).

**List of Figures**

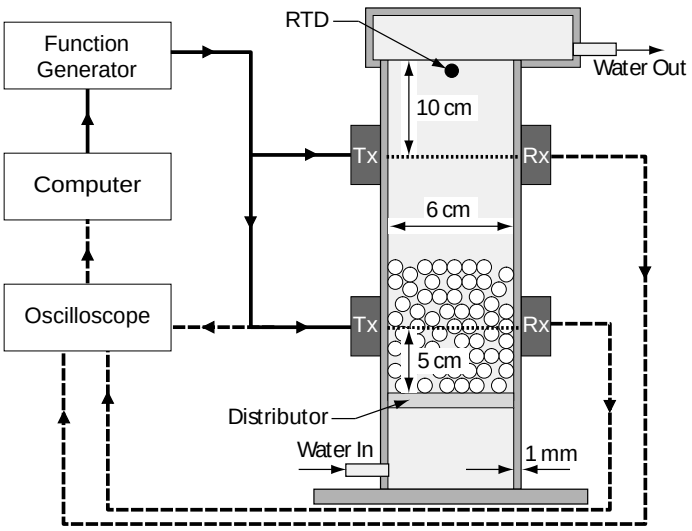


FIG. 1. A schematic diagram of the experimental apparatus is shown. Solid (dashed) lines denote the transmitted (received) electrical signal paths. The glass beads are not drawn to scale.

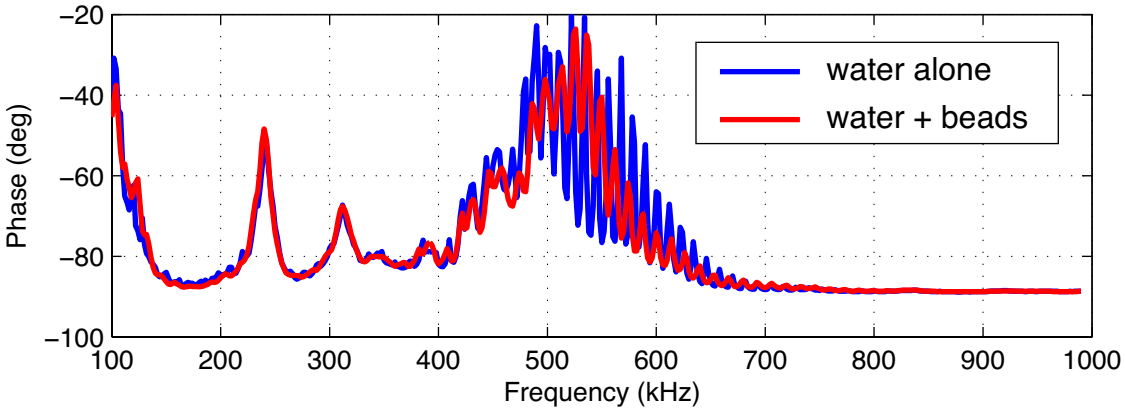


FIG. 2. (Color online) The phase of the measured electrical input impedance of one of the receiving transducers depicted in Fig. 1 is shown. The blue curve is for the transducer mounted in the apparatus when filled with water, and the red curve is for water-saturated beads. The phase difference apparent within the experimental frequency range (300 kHz through 800 kHz) was found to lead to correctable systematic errors in the sound speed measurement.

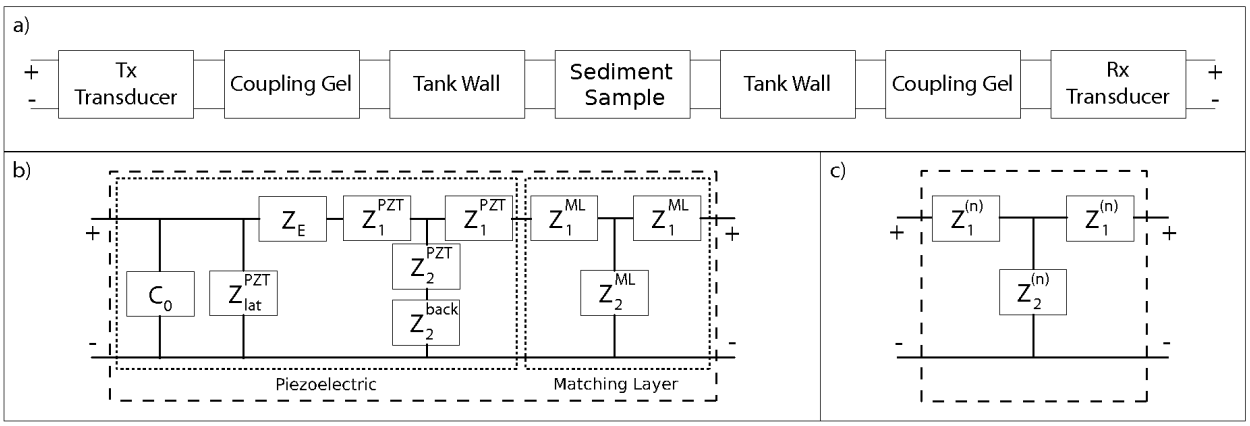


FIG. 3. A schematic of the transmission line model is shown in (a). It is composed of a Mason model for the transducers (b) and generic transmission line elements (c) for the remaining layers.

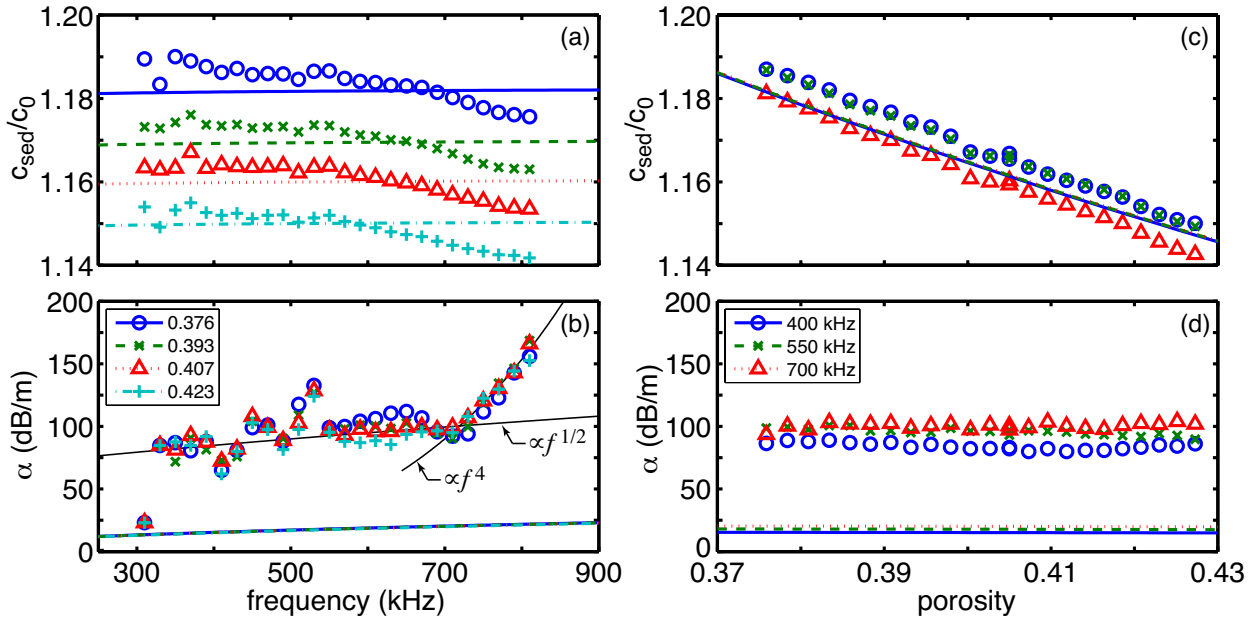


FIG. 4. (Color online) Measured sound speed ratios and attenuation coefficients of water-saturated glass beads are shown as a function of frequency in (a) and (b) and as a function of porosity in (c) and (d). Heavy dashed and solid lines correspond to the predictions of the EDFM[13] and symbols correspond to measurements. Trendlines are shown with light solid black lines in (b) to illustrate $f^{1/2}$ dependance below 700 kHz and $f^4$ dependance above.